Alteration of fossil-bearing shale (Autun, France; Permian), part II: Monitoring artificial and natural ageing by combined use of S and Ca K-edge XANES analysis, Rock-Eval pyrolysis and FTIR analysis

Giliane P. Odin, Frederik Vanmeert, François Farges, Georges Gand, Koen Janssens, Maria-Fernanda Romero-Sarmiento, Jean-Sébastien Steyer, Delphine Vantelon, Véronique Rouchon

Annales de Paléontologie 101 (2015) 225–239

Disponible en ligne sur
ScienceDirect
www.sciencedirect.com

Elsevier Masson France
EM|consulte
www.em-consulte.com

Original article

Alteration of fossil-bearing shale (Autun, France; Permian), part II: Monitoring artificial and natural ageing by combined use of S and Ca K-edge XANES analysis, Rock-Eval pyrolysis and FTIR analysis

Dégradation de schistes argileux fossilifères (Bassin d'Autun, France, Permien), partie II : vieillissements naturels et artificiels suivis par spectrométrie d'absorption au seuil de la raie K du soufre et du calcium, par pyrolyse Rock-Eval, et analyse IRTF

Giliane P. Odin[a,b], Frederik Vanmeert[c], François Farges[d], Georges Gand[e], Koen Janssens[c], Maria-Fernanda Romero-Sarmiento[f], Jean Sébastien Steyer[b], Delphine Vantelon[g], Véronique Rouchon[a,*]

[a] *Centre de Recherche sur la Conservation (CRC, USR 3224), Sorbonne Universités, Muséum national d'Histoire naturelle, Ministère de la Culture et de la Communication, CNRS, CP21, 36, rue Geoffroy-Saint-Hilaire, 75005 Paris, France*
[b] *Centre de Recherche sur la Paléobiodiversité et les Paléoenvironnements (CR2P, UMR 7207), Sorbonne Universités, Muséum national d'Histoire naturelle, Université Pierre et Marie Curie, CNRS, CP 38, 8, rue Buffon, 75005 Paris, France*
[c] *Department of Chemistry, University of Antwerp, Groenenborgerlaan 171, 2020 Antwerp, Belgium*
[d] *Institut de Minéralogie, de Physique des Matériaux et de Cosmochimie (IMPMC, UMR 7590), Sorbonne Université, Muséum national d'Histoire naturelle, CNRS, 61, rue Buffon, 75005 Paris, France*
[e] *Laboratoire Biogéosciences, (Université de Bourgogne, Centre National de la Recherche Scientifique) UMR-CNRS/uB 6282, 6, boulevard Gabriel, 21000 Dijon, France*
[f] *IFP Énergies nouvelles, Direction Géosciences, 1 et 4, avenue de Bois-Préau, 92852 Rueil-Malmaison cedex, France*
[g] *Synchrotron Soleil, L'Orme des Merisiers, Saint Aubin, BP48, 91192 Gif sur Yvette, France*

ARTICLE INFO

Article history:
Received 29 September 2014
Accepted 6 February 2015
Available online 26 March 2015

Keywords:
Shale
Fossil
Calcium
Sulfur
Oxidation
Organic matter
XANES
Pyrite
Rock-Eval Pyrolysis
Autun Basin

ABSTRACT

Fossil-bearing shale specimens that include sulfides in their compositions are chemically reactive and sometimes also mechanically fragile. This decay is often related to iron sulfate efflorescence resulting from the oxidation of sulfide compounds. The processes underlying these degradations are poorly known, thus impeding the elaboration of curative or preventive treatments. The present contribution aims to identify the origin of museum specimen alterations. It focuses on the Flouest collection housed at the Muséum National d'Histoire Naturelle (MNHN, Paris, France) and originating from the Autun Basin (Saône-et-Loire, France, Permian). To evaluate the alteration of MNHN specimens, it appeared necessary to compare their composition with that of unaltered shale so as to identify chemical changes occurring during ageing. Therefore, new material was collected in the Autun Basin, among others on the locality of Muse that corresponds to the same lithostratigraphic unit as that of the MNHN specimens. This material was, if necessary, artificially aged. The first part of this work, presented elsewhere, deals with the use of X-ray diffraction and Mössbauer spectroscopy for characterizing iron reactivity and speciation. It leads to the conclusion that the reactivity of iron in the shale matrix was limited and could not account for the large efflorescence of iron (II) sulfate occurring nearby the fossil. The second part presented here focuses on the use of S K-edge X-ray Absorption Near Edge Structure (XANES) spectroscopy for characterizing sulfur speciation and reactivity. Measurements were performed on the shale matrix and on thin layers of maceral found in the proximity of damaged areas. As sulfur may be found in association with calcium or organic matter, complementary techniques were implemented, such as FTIR spectroscopy, Rock-Eval

* Corresponding author.
E-mail addresses: giliane.odin@mnhn.fr (G.P. Odin), frederik.vanmeert@uantwerpen.be (F. Vanmeert), farges@mnhn.fr (F. Farges), georgesb.gand@orange.fr (G. Gand), koen.janssens@uantwerpen.be (K. Janssens), maria-fernanda.romero-sarmiento@ifpen.fr (M.-F. Romero-Sarmiento), steyer@mnhn.fr (J.S. Steyer), delphine.vantelon@synchrotron-soleil.fr (D. Vantelon), rouchon@mnhn.fr (V. Rouchon).

http://dx.doi.org/10.1016/j.annpal.2015.03.001

pyrolysis (characterization of organic matter content) and Ca K-edge XANES (analysis of calcium speciation) spectroscopy. It was shown that sulfur is mainly related to thioether, sulfoxide, iron sulfide, and sulfates whereas calcium is mainly bound to carboxylate, carbonate and/or sulfate groups. FTIR analysis of the macerals confirmed the presence of vitrinite on damaged MNHN specimens. The low oxygen content of new shale samples determined by Rock-Eval pyrolysis indicates that the organic matter is well preserved, despite the fact that samples come from outcrop surface. In the newly collected material, sulfur is mainly related to organic sulfides (thioether) with a minor occurrence of iron sulfide. In the shale fraction of damaged MNHN specimens, sulfur is mostly oxidized into a mixture of iron and calcium sulfate. However, in the vitrinite layers of the same specimens, a large proportion of sulfur corresponds to organic sulfides. Also the oxidation of sulfur does not occur homogeneously but preferentially in the shale fraction, probably because this latter is porous whereas vitrinite is not. Artificial ageing of new shale material showed that the oxidation of organic sulfides could be reproduced at 90 °C, 80% of relative humidity. However, the obtained efflorescence almost exclusively corresponds to calcium sulfate whereas iron (II) sulfates are mostly observed on MNHN specimens. The new material collected on site is probably to be questioned, and future studies will have to select new samples with fossil remains. This will be the object of the third part of this work.

Mots clés :
Argilite
Schiste
Fossile
Calcium
Soufre
Oxydation
Matière organique
XANES
Pyrite
Pyrolyse Rock-Eval
Bassin d'Autun

RÉSUMÉ

Les schistes argileux fossilifères qui incluent des sulfures dans leur composition sont chimiquement réactifs et deviennent aussi parfois fragiles mécaniquement. Ces dégradations sont souvent liées à des efflorescences de sulfates de fer (II) résultant de l'oxydation de produits sulfurés. Les mécanismes sous-jacents à ces dégradations sont généralement peu connus, ce qui limite l'élaboration de traitements curatifs ou préventifs. Ce travail vise à identifier l'origine de la dégradation de spécimens de collections, en particulier ceux de la collection Flouest qui provient du Bassin d'Autun (Saône-et-Loire, France, Permien) et est aujourd'hui conservée au Muséum national d'Histoire naturelle (MNHN). Pour évaluer la dégradation des spécimens MNHN, il est apparu nécessaire de comparer leur composition à celles de schistes argileux non altéré, de manière à mettre en évidence les changements de composition chimique. C'est pourquoi du matériel neuf a été prélevé dans le Bassin d'Autun, entre autres sur le site de Muse qui correspond à la même unité lithostratigraphique que celle des spécimens MNHN. Ce matériel est, au besoin, vieilli artificiellement. La première partie de ce travail, présentée ailleurs, porte sur l'utilisation conjointe de la diffraction des rayons X et de la spectrométrie Mössbauer pour caractériser la spéciation et la réactivité du fer dans la matrice argileuse. Il s'avère que la réactivité du fer est limitée et ne permet pas d'expliquer des larges efflorescences de sulfates de fer (II) qui apparaissent à proximité des fossiles. La seconde partie de ce travail porte sur l'utilisation de la spectrométrie d'absorption au seuil de la raie K du soufre pour caractériser la spéciation du soufre et sa réactivité. Les mesures ont été menées sur la matrice argileuse et sur les fines couches de macéraux présentes à proximité des efflorescences. Comme le soufre peut être associé au calcium et à la matière organique, des techniques analytiques complémentaires ont été mises en œuvre, comme la spectrométrie IRTF, la pyrolyse Rock-Eval (pour l'analyse de la matière organique) et la spectrométrie d'absorption au seuil de la raie K du calcium (pour la spéciation du calcium). Il a été montré que le soufre s'apparente principalement à des thioethers, des sulfoxydes, des sulfures de fer et des sulfates alors que le calcium est principalement lié à des groupements carboxylates, carbonates et sulfates. L'analyse IRTF des macéraux confirme la présence de vitrinite sur les spécimens endommagés. La teneur en oxygène déterminé par pyrolyse Rock-Eval sur les échantillons de schistes prélevés sur site, indique que la matière organique est bien préservée, malgré le fait que les échantillons proviennent de la surface d'affleurement. Dans le matériel nouvellement collecté, le soufre s'apparente principalement à des sulfures organiques (thioethers) avec une faible proportion de sulfures de fer. Dans la matrice des spécimens MNHN endommagés, le soufre est presque entièrement oxydé en un mélange de sulfates de fer et de calcium. Cependant, dans la vitrinite de ces mêmes spécimens, une large proportion de soufre correspond à des sulfures organiques. Ainsi, l'oxydation du soufre n'intervient pas de manière homogène dans le matériau, mais de manière préférentielle dans la partie schisteuse, probablement du fait que celle-ci est poreuse alors que la vitrinite ne l'est pas. Le vieillissement artificiel du matériel nouvellement prélevé montre qu'il est possible de reproduire l'oxydation des sulfures organiques à 90 °C et 80 % d'humidité relative. Cependant les efflorescences obtenues correspondent quasi exclusivement à des sulfates de calcium alors que ce sont des sulfates de fer (II) qui sont observés sur les spécimens MNHN. Le matériel nouvellement collecté doit probablement être remis en question, en particulier en choisissant des échantillons contenant des restes fossiles. Cette démarche fera l'objet de la troisième partie de ce travail.

1. Introduction

Sulfides are important constituents of fossils. Their oxidation can induce irreversible damage to paleontological collections. Indeed, when exposed to air and moisture, sulfides can be oxidized as sulfates. These may undesirably recrystalize as sulfate efflorescence, thus seriously compromising long-term conservation of fossils. Those phenomena are visible on fossil shale originating from the Autunian of the Autun Basin and currently housed at the Muséum National d'Histoire Naturelle (MNHN, Paris, France) (Rouchon et al., 2012).

Intensive research was dedicated to the decay of pyrite, which is one of the most common iron sulfide (Rimstidt and Vaughan, 2003; Rosso and Vaughan, 2006; Murphy and Strongin, 2009; Chandra

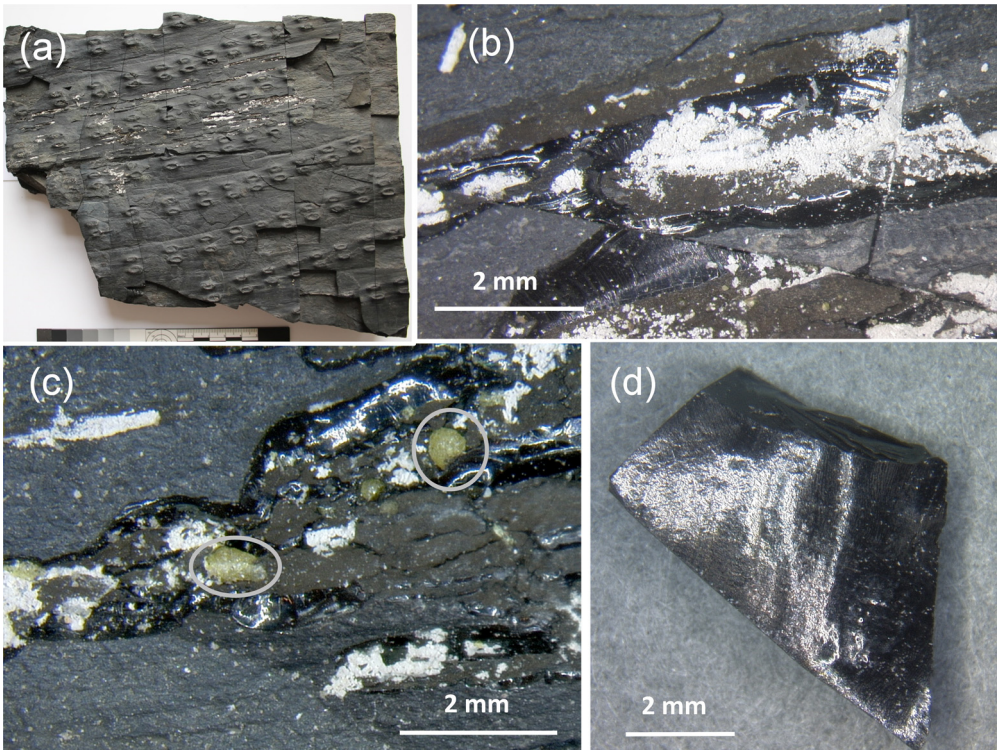

Fig. 1. Specimen MNHN.F.6889; (a) general view; (b, c) detail of a damaged area showing white crystals of rozenite ($Fe^{II}SO_4{\cdot}4H_2O$), szomolnokite ($Fe^{II}SO_4{\cdot}H_2O$) and yellow crystals of ferricopiapite ($Fe^{III}_{2/3}Fe^{III}_4(SO_4)_6(OH)_2{\cdot}20H_2O$) (grey circle) on a glossy black layer of maceral; (d) sample 6889-maceral.
Spécimen MNHN.F.6889 ; (a) Vue générale ; (b, c) détail d'une zone endommagée montrant des cristaux blancs de rozénite ($Fe^{II}SO_4{\cdot}4H_2O$), de szomolnokite ($Fe^{II}SO_4{\cdot}H_2O$) et des cristaux jaunes de ferricopiapite ($Fe^{III}_{2/3}Fe^{III}_4(SO_4)_6(OH)_2{\cdot}20H_2O$) (cercles gris) sur une couche brillante et noire de macéral ; (d) échantillon 6889-maceral.

and Gerson, 2010; Schoonen et al., 2010; Heidel and Tichomirowa, 2011). In comparison, limited research has been conducted on pyritized fossils (Howie, 1977; Newman, 1998; Fellowes and Hagan, 2003) whose composition is even more complex than that of pyrite crystals. Fossils in particular may contain other reactive sulfides. Thus the degradation of pyritized fossils is not limited to pyrite decay but may concern a larger panel of sulfides (inorganic and organic) as well. A better understanding of the degradation of these materials is of primary importance for managing the long-term conservation of paleontological collections.

Autunian shale layers of the Autun Basin (Saône-et-Loire, France; Permian) were mined until the 1960s to produce oil and ammonium sulfate (Chabard and Passaqui, 2006). They contain organic matter and reduced (organic or mineral) sulfur compounds. The study presented here deals with MNHN specimens originating from these layers. It more specifically focuses on the Flouest fossil collection housed at the MNHN that was collected in the 19th century on the locality of Le Ruet (Tavernay, Saône-et-Loire, France). This collection comprises several damaged specimens of which the conservation report has previously been published (Rouchon et al., 2012). Damage consists in iron sulfate efflorescence growth outlining the fossil shape. This efflorescence compromises the fossil legibility and the integrity of the matrix. Additionally, it is often observed that sulfate efflorescence growth had occurred nearby maceral layers (Figs. 1–3). Notably, no pyrite or iron sulfide is noticeable under a stereo microscope.

This study was undertaken in order to better understand the cause of the above mentioned degradation and in particular to identify the reactive species that were initially present before the specimens got deteriorated. The occurrence of iron sulfate efflorescence directly questions the speciation of iron and sulfur in shale. It was also found necessary to follow the evolution of shale material after excavation by analytical techniques that enable iron and sulfur characterization. This approach is a prerequisite for identifying damaging phenomena. It is expected to help in defining appropriate preservation conditions for damaged specimens, and also in comprehending the risk of damage related to similar paleontological material that is currently excavated.

This work was organized in three parts. In the first part (Odin et al., 2015), new samples of shale originating from the Autun Basin (Saône-et-Loire, France, Permian) were characterized by X-ray diffraction, Mössbauer spectroscopy, porosimetry and permeability measurements. These analyzes showed that there is a minor occurrence of pyrite. Iron is mostly correlated to the clay fraction of shale. Porosity measurements showed that shale porous network is limited (7 to 10% v/v) and narrow (average radius from 3 to 7 nm). Moreover, shale exhibits a low transverse permeability to water vapor and no permeability to air. As a result, iron sites are poorly accessible to water and not at all to oxygen, except in cleavage plans. Similar analysis performed on the shale fraction of damaged specimens of the Flouest collection that were collected in the 19th century showed that pyrite is largely transformed into sulfates (jarosite and gypsum were identified). This oxidation, mainly correlated to water vapor transfer, can however not explain the large efflorescence observed nearby the fossil. Indeed, jarosite and gypsum are poorly water soluble. Once formed, they remain in the inner part of the shale without inducing obvious damage. The cause of damage should also be researched close to the efflorescence. Damage is believed to occur locally on specific spots that initially comprised reactive compounds.

The second part of this study, presented here, aims to determine the sulfur speciation through S K-edge X-ray Absorption Near Edge Structure (XANES) spectroscopy, a technique commonly used in geochemistry (Sarret et al., 2002; Prietzel et al., 2003; Mikhlin and Tomashevich, 2005; Van Hullebusch et al., 2009; Almkvist

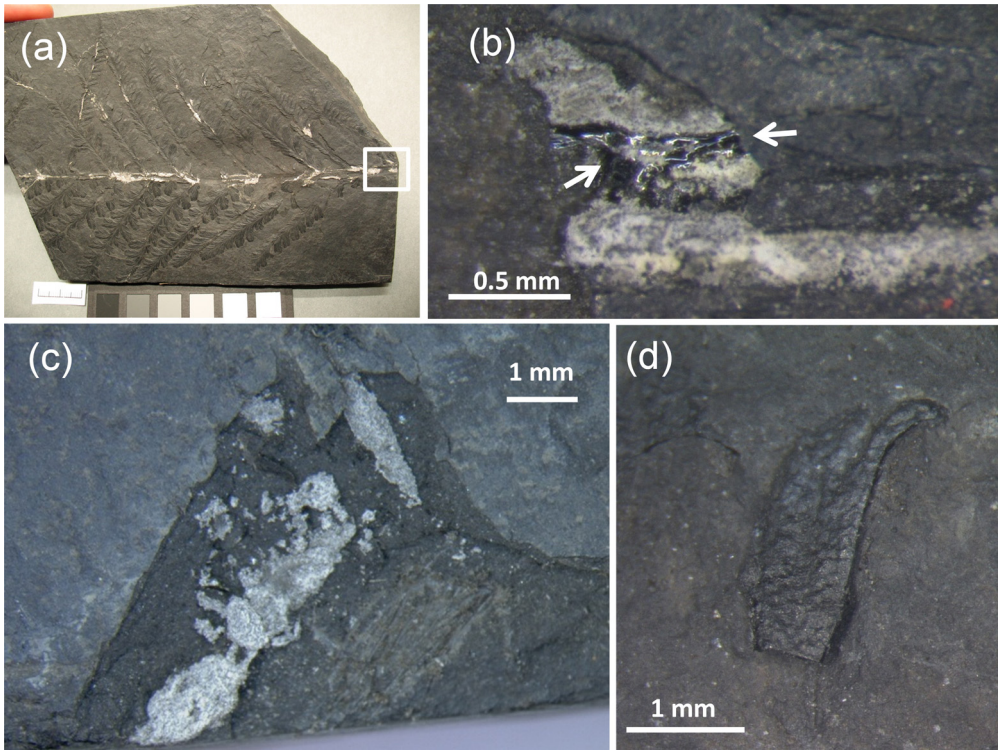

Fig. 2. Specimen MNHN.F.6888; (a) general view; (b) detail of a damaged area showing white crystals of rozenite and szomolnokite next to thin shiny layers of black maceral (white arrows); (c) example of a detached flake provoked by efflorescent crystal growth of rozenite; (d) sample 6888-leaf.
Spécimen MNHN.F.6888 ; (a) vue générale ; (b) détail d'une zone endommagée montrant des efflorescences blanche de rozénite et de szomolnokite à proximité d'une couche fine et brillante de macéral noir (flèches blanches) ; (c) exemple de détachement d'un fragment provoqué par la croissance d'efflorescences de rozénite ; (d) échantillon 6888-leaf.

et al., 2010; Boye et al., 2011; Manceau and Nagy, 2012). S K-edge XANES in particular makes it possible to identify organic sulfides versus inorganic sulfides, and to monitor the oxidation of sulfur versus ageing, two aspects that are of primary importance to understand the degradation processes taking place in shale fossils. Analysis of the shale fraction of damaged specimen of the Flouest collection highlighted a significant amount of calcium sulfate. Therefore, Ca K-edge X-ray Absorption Near Edge Structure (XANES) spectroscopy was additionally undertaken on some samples in order to determine the original speciation of calcium. This approach was usefully complemented by FTIR analysis and Rock-Eval pyrolysis for the characterization of organic matter content.

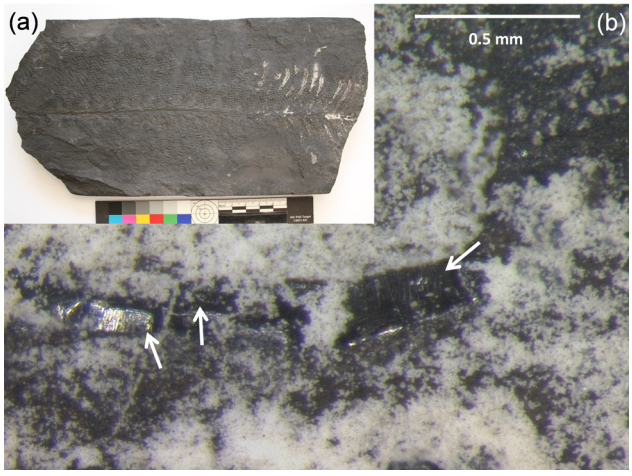

Fig. 3. Specimen MNHN.F.6892; (a) General view; (b) detail of a damaged area showing rozenite and szomolnokite crystals next to thin layers of maceral (white arrows);.
Spécimen MNHN.F.6892 ; (a) Vue générale ; (b) détail d'une zone endommagée montrant des efflorescences de rozénite et de szomolnokite à proximité d'une couche de macéral (flèches blanches).

2. Samples and geological settings

2.1. Specimens from the Flouest collection

Three specimens (MNHN.F.6888, MNHN.F.6889 and MNHN.F. 6892) from the Flouest collection (MNHN) were chosen for analysis because they present typical cases of degradation observed in this investigated collection. For simplicity, they will hereafter be referred to as 6888, 6889 and 6892 respectively. These specimens originate from the locality of "Le Ruet", in the Autun Basin and jointly entered the Museum collection in 1865. They are currently stored in the same drawer, in a room with no air conditioning. The variations in temperature and humidity occurring in this room were previously reported (Odin et al., 2014).

The identification and conservation report of these fossils can be found elsewhere (Rouchon et al., 2012). The three specimens are severely damaged by crystalline efflorescence outlining the fossil. This efflorescence is related to iron (II) sulfates (rozenite, $Fe^{II}SO_4{\cdot}4H_2O$ and szomolnokite, $Fe^{II}SO_4{\cdot}H_2O$) with, in the case of sample 6889, some small amount of ferricopiapite ($Fe^{III}{}_{2/3}Fe^{III}{}_4(SO_4)_6(OH)_2{\cdot}20H_2O$).

Specimen 6889 (Fig. 1a) comprises of a 0.5 to 1 cm thick layer of maceral supported by the shale (Fig. 1c). On the two other specimens, 6888 and 6892 (Figs. 2a and 3a), a thin layer of maceral is observed at the border of the stem, next to crystalline efflorescence (Figs. 2b,c and 3b,c, white arrows).

Two samples of macerals (hereafter referred to as 6889-maceral and 6892-maceral) were taken for analysis: (i) on specimen 6889,

Table 1
List of damage visually observed on artificially aged samples.
Liste des dommages observés visuellement sur les échantillons vieillis artificiellement.

Site	Ageing conditions	Efflorescence	Cracks	S K-Edge XANES spectrum (Fig. 5)
Muse FL	40 °C, 50% RH	No	Yes	f
	40 °C, 80% RH	Yes	Yes	i
	90 °C, 50% RH	Yes	No	j
	90 °C, 80% RH	Yes	No	k
Surmoulin	40 °C, 50% RH	No	Yes	g
	90 °C, 50% RH	Yes	No	h

the maceral forms a thick layer, enabling sampling from a well preserved area (no visible efflorescence) (Fig. 1d); (ii) on specimen 6892, the sample was obtained from a damaged area of the stem as it was not possible to sample in the well preserved part of the fossil.

On specimen 6888, it was impossible to sample maceral without damaging the fossil. On this fossil however, some leaves were flaking away. Their aspect is similar to that of the shale, yet with a slightly enhanced gloss and smoothness. One of them (Fig. 2d), most part of which was missing, was taken for analysis and hereafter referred to as 6888-leaf.

On the three fossils, the shale portion was additionally sampled and hereafter referred to as 6888-shale, 6889-shale and 6892-shale.

2.2. Newly excavated shale samples

2.2.1. Shale samples from the locality of Muse

In order to reproduce damage in laboratory conditions, it was intended to sample new shale material with petrographic characteristics similar to those of damaged specimens. Unfortunately, the mine of Le Ruet (Tavernay, Saône-et-Loire, France), which probably yielded the MNHN specimens, is no longer accessible. We opted for an alternative outcrop with the same lithostratigraphic unit (i.e., the bedding of Muse, "Autunian" of the Autun Basin): the outcrop of Muse (Dracy Saint Loup, Saône-et-Loire, France), located approximately 6 km from the locality of Le Ruet, was therefore chosen. This choice was also motivated by the fact that the site is currently open for paleontological fieldwork (Gand et al., 2010).

The "Autunian" of the Muse outcrop comprises several layers, the most famous of which is commonly called the "Muse fish layer" and hereafter referred to as *Muse FL*. This layer (Late Carboniferous – Lower Permian of the Autun Basin) is located at the base of the bedding of Muse above a pebble layer (Lally Sandstones). Since the 19th century, the *Muse FL* yielded hundreds of *Actinopterygii* specimens (mostly Aeduellidae) now spread in many museum collections and in various conditions of conservation. Specimens found in this layer are of exceptional preservation. They are currently collected for research and exhibition purposes. A better knowledge of their composition and stability versus time will certainly help in monitoring their future preservation in museum collections.

2.2.2. Shale samples from the locality of Surmoulin

In a previous study (Odin et al., 2014), samples were taken from different outcrops of the Autun Basin to carry out artificial ageing experiments. Among these, samples from the Surmoulin layer (outcrop of Surmoulin, Dracy Saint Loup, Saône-et-Loire, France) were the most reactive: they showed large calcium sulfate efflorescence and substantial mechanical damage versus artificial ageing. It was also found relevant to investigate this material, hereafter referred to as *Surmoulin*.

2.2.3. Cautions taken during shale sampling

The site of Muse is located in the embankment of a road and that of Surmoulin in the embankment of a river, meaning that the samples were collected close to the surface and were exposed to weathering. When split, they showed orange rust-colored areas. Black areas, expected to have been less subjected to weathering, were chosen for analysis and in-laboratory artificial ageing. After excavation, the samples were isolated in anoxic conditions in order to limit drying and oxidation processes: they were placed in air and water tight plastic bags (ESCAL© film, Long Life for Art, Germany) with oxygen scavenger bags (ATCO© FTM absorbers, Long Life for Art, Germany).

2.2.4. Artificial ageing

Artificial ageing is commonly used in conservation science to reproduce the degradation of several types of homogeneous organic materials on which Arrhenius law is applicable (paper, plastics etc.). In the case of shale, which shows an anisotropic structure made of several sedimentary deposits, the use of artificial ageing for reproducing the alterations encountered on specimens is questionable. Alteration phenomena are not only governed by chemical reactions but also by diffusion of reactive species in the shale matrix and by crystalline growth mechanisms. Yet, artificial ageing remains the only available tool to study degradation pathways in a reasonable time. It was experimented in a previous study (Odin et al., 2014) on a large set of 168 samples (excluding the *Muse FL* samples) collected from different outcrops of the Autun Basin. Close to ambient conditions were used (50% RH, 40 °C) as well as more drastic ones (50% RH, 90 °C), for a duration of 15 weeks. Many of the samples exposed to 40 °C showed mechanical damage (cracks) while no crystalline efflorescence was visible. In contrast, most samples exposed to 90 °C showed crystalline efflorescence of gypsum but were not much affected by mechanical damage.

Two samples of Surmoulin were selected for this study from these first ageing experiments for they were perfectly illustrating the behavior mentioned above (Table 1). Complementary ageing experiments were undertaken for 15 weeks on *Muse FL* samples using similar conditions and also a higher humidity conditions (80% RH) in order to promote the degradation. Four *Muse FL* samples were chosen from this latter experiment for they showed efflorescence and/or cracks (Table 1).

3. Analytical methods

3.1. Rock-Eval pyrolysis

Rock-Eval pyrolysis has been extensively used for oil and gas exploration purposes in order to identify the type and the thermal maturity level of organic matter of both reservoir and source rocks present in sedimentary basins (Espitalié et al., 1985a,b, 1986; Behar et al., 2001). This technique consists in heating a small amount of sample (100 mg of ground shale or 50 mg of isolated kerogen) firstly in an inert atmosphere (pyrolysis), then secondly in aerated conditions (oxidation). Rock-Eval pyrolysis enables the acquisition of different parameters (S1, S2, S3 and T_{max}, among others) that are used for the calculation of the total organic carbon (TOC) content, the total mineral carbon (MINC) content, the hydrogen index (HI) and the oxygen index (OI).

Today, it is widely accepted that the presence of a mineral matrix could sometimes affect the Rock-Eval parameters obtained by pyrolysis of sedimentary organic matter (Espitalié et al., 1985a; Peters, 1986). This effect can be considerable for samples containing clays that retain hydrocarbons, thus provoking a decrease of the S2 signal and consequently an underestimation of HI (Espitalié et al., 1985a; Peters, 1986). In order to evaluate the impact of the mineral matrix, kerogen samples were isolated from shale using acid treatments (Durand and Nicaise, 1980).

All Rock-Eval analyses were performed on a Rock-Eval 6 device operating at IFP Energies Nouvelles (France), using the "IFP Basic/Bulk-Rock method" temperature program for source rocks and the "IFP Pure Organic Matter method" for isolated kerogen. The experimental data regarding these methods are available elsewhere (Behar et al., 2001). All measurements were duplicated or triplicated.

3.2. Fourier Transform Infrared spectroscopy (FTIR)

FTIR analyses were performed on a conventional spectrometer (Nicolet 6700, Thermo Fisher Scientific) equipped with a diamond Attenuated Total Reflectance (ATR) module (SMART endurance). Destructive analyses were conducted as follows: a sample grain was placed on the ATR module, then crushed within a fraction of second and pressed against the diamond during the analysis by the use of an articulated arm. Spectra were acquired by 60 scans within the range 4000 cm^{-1}–525 cm^{-1} and were processed with the OMNIC software (Thermo Fisher Scientific).

3.3. X-ray Absorption Near Edge Structure (XANES) spectroscopy

Calcium (Ca) and sulfur (S) K-edge XANES spectra were collected on the LUCIA beamline (SOLEIL synchrotron source, France). Measurements were performed in fluorescence mode with the sample surface rotated 20° with respect to the incident beam while the detector was oriented perpendicular to the incident beam. Spectra were normalized and treated with the Demeter package (Ravel and Newville, 2005) using a linear combination of several carefully chosen model compounds. These linear combinations were compared with those obtained from Continuous Cauchy Wavelets Transforms (CCWT) (Munoz et al., 2003) of the normalized XANES spectra.

CCWT are time-frequency wavelets decompositions, i.e., for XAFS/XANES signals, a *k*-space vs. R-space decomposition. *k* is the photoelectron wavenumber (here in the range 0 to 6.5 $Å^{-1}$). It is correlated to the scanning energy. The R + Δ parameter corresponds to the uncorrected interatomic phase-shifts S–X distance where X is one of the various neighbors around the absorbing S (the backscattering phase shift correction Δ was not determined in this work). Each Δ*k*-space segment corresponds to a ΔR-space segment resulting in a CCWT modulus, also referred to as the wavelet magnitude. This magnitude is displayed versus *k* and R + Δ as a 2D-colormap, with intensities ranging from 0 (black) to its maximum (white). The CCWT treatment allows plotting EXAFS or XANES data in three dimensions (*k*, R + Δ, and the CCWT modulus) and is therefore more informative than Fourier transforms (FT) spectra alone even when spectral artifacts are present, such as multiple-scattering features, multi-electronic excitations, or noise. Moreover, this method provides important information concerning the *k* range of each EXAFS/XANES contribution, such as next nearest-neighbors identification.

S K-edge XANES spectra were collected with an acquisition time of 1 second per point in the energy range from 2450 to 2540 eV, with a special emphasis in the edge region: 0.2 eV steps between 2460.2 eV and 2490 eV, 1 eV steps between 2491 and 2510 eV and 2 eV steps below 2460 eV and above 2510 eV. In order to reduce the signal-to-noise ratio and to limit unwanted sulfur photo-reduction induced by the X-ray beam, all analyses were performed using a defocused beam (1.5 × 1 mm) thus reducing the incident photon flux per surface unit. The energy scale was calibrated by measuring the position of the main resonance ("white line") of gypsum set at 2482.5 eV.

Ca K-edge XANES spectra were recorded with an acquisition time of 1 second per point in the energy range from 4000 to 4200 eV using 0.2 eV steps between 4036.2 eV and 4068 eV, 0.5 eV steps between 4068.5 and 4080 and 2 eV steps before 4036 eV and after 4080 eV. All analyses were performed with a defocused beam. No beam-induced change of the samples (photo-reduction, etc.) was observed. The energy scale was calibrated by measuring the position of the main resonance (white line) of gypsum ($CaSO_4{\cdot}2H_2O$) set at 4050.4 eV.

Several model compounds were considered in this study. They were purchased from Sigma Aldrich, with the exception of four minerals of natural origin: pyrrhotite from Morrovehlo, Brasil (MNHN, MIN.2009.22263, confirmed by X-ray diffraction), pyrite from an unknown location, Mexico (personal collection, confirmed by X-ray diffraction), solid asphalt from Chapopati, Palenque, Mexico (MNHN, GI37) and crude-oil from deposit 28, Richemont, Alsace, France (MNHN, GI collection).

Maximal caution was taken in the preparation of the un-aged shale samples in order to insure that the analyzed surfaces were not exposed to oxygen: these samples were placed in an oxygen free glove box (below 10 ppm oxygen), split to obtain a new surface and transferred in an oxygen free transfer vessel from the glove box to the analyzing vacuum chamber (2 10^{-2} atm). Preliminary testing showed that the oxygen free transfer was not necessary to implement, as no significant sulfur oxidation was detected on un-aged shale samples that had been exposed to oxygen for several hours. It was therefore decided to prepare all shale samples in the same way as mentioned above, yet without using the oxygen free sample passing system. Samples were instead placed in air tight containers during their transfer from the glove box to the vacuum analyzing chamber (2 10^{-2} atm). This approach was easier to implement and guaranteed no oxidation side effects on the samples as they were exposed to oxygen for a few seconds only.

In a previous study, it was attempted to measure the amount of sulfur present in *Muse FL* and *Surmoulin* shale with a CHNS analyzer (Odin et al., 2015). Yet, this element is present at too low concentration (< 0.5% w/w) to allow for its detection or quantification by this technique. Therefore in this study, the amount of sulfur (and calcium) was quantified on some chosen samples by the step edge method taking advantage of the high sensitivity of the synchrotron fluorescence probe.

4. Results

4.1. Rock-Eval pyrolysis

Rock-Eval results from both shale and corresponding isolated kerogen are shown in Table 2. The TOC values of investigated shale samples range between 8.2 and 11.9% w/w. In general, for shale samples, the HI, OI and T_{max} values vary between 461 to 600 mg(HC)·g^{-1}(TOC), 3 to 43 mg(HC) g^{-1}(CO_2) and 421 to 432 °C, respectively. Actually, based on Rock-Eval data, *Surmoulin* and *Muse FL* shale samples have a relatively homogeneous composition (with respect to the intrinsic heterogeneous nature of sedimentary geological samples) and present similar features with values of S2, S3, S4CO2, S3CO, and S4CO in the range of 38 to 69 mg(HC)·g^{-1}, 0.3 to 3.5 mg(CO_2)·g^{-1}, 143 to 176 mg(CO_2)·g^{-1}, 0.5 to 1.1 mg(CO)·g^{-1} and 11.9 to 36.4 mg(CO)·g^{-1} respectively. These values are consistent with previous measurements performed in the Autun Basin (Marteau, 1983).

Table 2
Rock-Eval data measured on un-aged shale samples and corresponding kerogens.
Données Rock-Eval mesurées sur les échantillons de schiste bitumineux non vieillis et sur leurs kérogènes.

			Shale samples (BR)					Kerogen samples (KD)				
			Surmoulin		Muse FL			Surmoulin		Muse FL		
Date of excavation			Sept. 2012		Sept. 2012			Sept. 2012		Sept. 2012		
Date of analysis			Jan. 2014		Jan. 2014			Sept. 2014		Sept. 2014		
Unit	**Rock-Eval parameter**	**Definition**	*1*	*2*	*1*	*2*	*3*	*1*	*2*	*1*	*2*	*3*
mg(HC)·g^{-1}	S1	Free hydrocarbons	2.5	3.4	1.5	1.1	0.6	22.5	27.8	12.8	12.8	15.0
	S2	Oil potential	54	62	69	57	38	512	534	441.8	417	405
mg(CO2)·g^{-1}	S3	CO2 (pyrolysis) organic	1.3	0.7	0.3	0.6	3.5	8.9	5.8	3.3	3.8	21.6
	S3′	CO2 (pyrolysis) mineral	12.5	10.2	0.8	1.9	3.9	28.7	16.9	17.3	13.5	32.4
	S4CO2	CO2 (oxidation) organic	144	149	167	176	143	1045	997	937	1038	1016
mg(CO)·g^{-1}	S3CO	CO (pyrolysis) organic	0.7	0.5	0.6	0.5	1.5	8.7	6.3	4.9	5.9	16.1
	S3′CO	CO (pyrolysis) organic and mineral	0.5	0.6	0.5	1.1	0.6	30.6	17.1	17.9	17.8	20.4
	S4CO	CO (oxidation) organic	11.9	17.9	34.3	36.4	21.1	162	235	181	207	251
°C	T_{max}	Temperature of peak S2 max (shale)	422	421	432	429	421	421	420	432	429	423
% (C) w/w	TOC	Total organic carbon	9.2	10.3	11.9	11.2	8.2	82.5	85.5	72.6	74.4	76.3
	MINC	Total mineral carbon	4.0	3.6	0.0	0.1	0.1	–	–	–	–	–
mg(HC)·g^{-1}(TOC)	HI	Hydrogen index (shale)	587	600	577	505	461	620	624	609	561	530
mg(CO2)·g^{-1}(TOC)	OI	Oxygen index (shale)	14	7	3	5	43	11	7	5	5	28

The HI versus T_{max} and OI values measured on shale and kerogen samples are gathered in Fig. 4. The values of OI and HI obtained on source rocks are slightly underestimated but still similar to those obtained on isolated kerogen. The highest deviation, observed on sample 3 of *Muse FL*, remains moderate. Also Rock-Eval parameters are relatively similar for shale and kerogen samples, meaning that there is no significant influence of the mineral matrix. This is accounted to the fact that *Surmoulin* and *Muse FL* shale samples show a relatively high organic matter content.

The main difference that was found in the two investigated layers corresponds to the total mineral carbon content (MINC). Significant amounts of MINC (from 3 to 4% w/w) in the *Surmoulin* samples are consistent with the detection of dolomite by X-ray diffraction (Odin et al., 2015). In contrast, in *Muse FL* shale samples, the amount of the total mineral carbon is very low (< 0.1% w/w).

4.2. FTIR analysis

4.2.1. Maceral samples

The sample 6889-maceral derives from woody tissue of a *Syringodendron sp.* tree and should therefore be related to vitrinite. This is confirmed by FTIR analysis (Fig. 5, spectrum a) which shows characteristic features already reported in the literature (Chen et al., 2012; Li et al., 2013), in particular: (i) a medium to strong absorbance of the aliphatic C-H stretching mode at 2920 and 2850 cm^{-1}; (ii) a medium absorbance of the aromatic carbonyl/carboxyl C = O stretching mode at 1700 cm^{-1}; (iii) a strong absorbance of the aromatic C = C stretching mode at 1597 cm^{-1}; (iv) a strong absorbance of the aliphatic CH bending mode at 1450 cm^{-1}; (v) a medium absorbance of the aliphatic CH_3 bending mode at 1370 cm^{-1}; and (vi) a significant absorbance of the aromatic C-H out-of-plane bending at 867 cm^{-1} (one isolated aromatic CH group), 813 cm^{-1} (two or three adjacent aromatic CH groups) and 748 cm^{-1} (four adjacent aromatic CH groups).

The above mentioned features are also present in the FTIR spectrum of the sample 6892-maceral (Fig. 5, spectrum b). This sample, mainly composed of maceral organic matter, was taken from a damaged area rich in efflorescence. It may also contain degradation by-products. In particular, the peak at 1700 cm^{-1} (C = O) is more pronounced showing oxidation of organic matter. Sulfates are additionally present, as attested by additional absorption peaks attributed to gypsum ($CaSO_4{\cdot}2H_2O$, 3530 cm^{-1}, 3400 cm^{-1}, 1620 cm^{-1}, and 1104 cm^{-1}) and possibly jarosite ($KFe^{III}{}_3(OH)_6(SO_4)_2$, 1082 cm^{-1}, 1002 cm^{-1}), a phase already identified on this fossil (Rouchon et al., 2012). The large absorption band in the range 1000-1150 cm^{-1} may also find other interpretations: C-O stretching mode of alcohol; sulfates such as rozenite ($FeSO_4{\cdot}4H_2O$, 1620 cm^{-1}, 1070 cm^{-1}); or eventually sulfonates. All these features are related to oxidation phenomena. Also sample 6892-maceral is more damaged than sample 6889-maceral.

4.2.2. Shale samples

FTIR spectra of newly excavated shale samples and shale fractions of damaged specimen show many similarities (Fig. 5, spectra d to h), consistent with the fact that shale is mainly composed of quartz, kaolinite, illite, and vermiculite (Odin et al., 2015). Based on previous studies (Van der Marel and Krohmer, 1969; Elsass Damon, 1977; Sayin and Grafvonreichenbach, 1979; Post and Borer, 2002), the shale FTIR peaks were assigned as follows: (i) 3692 cm^{-1}, 3617 cm^{-1}, 910 cm^{-1} and 748 cm^{-1}: kaolinite; (ii) 3650 cm^{-1}: clay minerals, such as kaolinite, illite, or vermiculite; (iii) 936 cm^{-1} and 822 cm^{-1}: illite or vermiculite; (iv) 797 cm^{-1}, 775 cm^{-1} and the strong absorption near 1070 cm^{-1}: quartz; (v) 690 cm^{-1}: kaolinite or quartz.

The *Surmoulin* un-aged sample additionally exhibits a large absorption band around 1440 cm^{-1}, and narrow peaks at 877 cm^{-1} and 727 cm^{-1} that are not observed in any other spectra. These features are attributable to dolomite, consistent with X-ray diffraction measurements (Odin et al., 2015) and the Rock-Eval analysis that evidenced approx. 3.6 to 4% of mineral carbon on *Surmoulin* shale samples.

Finally, the presence of organic matter becomes visible on highly magnified FTIR spectra (Fig. 4, grey rectangle) at 2920 and 2850 cm^{-1} (aliphatic C-H stretching), 1620 cm^{-1} (C = C stretching), and in the region 1430–1450 cm^{-1} (aliphatic C-H bending and possibly NH stretching (Petit et al., 2006).

4.2.3. Sample 6888-leaf

The spectrum of sample 6888-leaf (Fig. 5, spectrum c) corresponds to a combination of 6892-maceral and 6888-shale spectra (Fig. 5, spectra b and d). As a result, sample 6888-leaf can be seen as a fraction of shale that is richer in organic matter than the matrix. This organic matter is substantially oxidized as attested by the absorption at 1700 cm^{-1}. Moreover, the sample contains gypsum

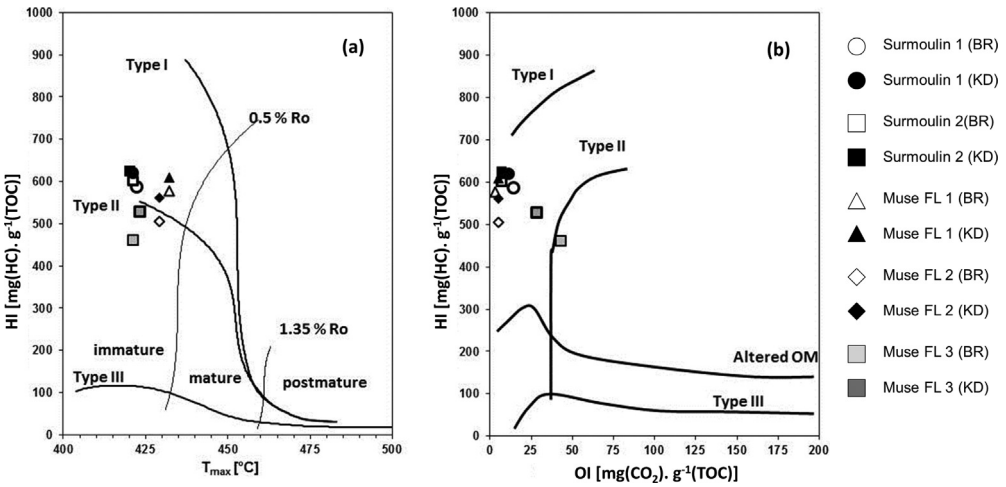

Fig. 4. HI vs. T_{max} diagram (a) and HI vs. OI diagram (b) of *Muse* and *Surmoulin* samples (type lines modified from Espitalié et al., 1986). BR: shale; KD: kerogen.
Représentation des échantillons de Muse et Surmoulin sur un diagramme HI en fonction de T_{max} (a) et HI en fonction de OI (b) (les lignes séparant les types s'inspirent de Espitalié et al., 1986). BR : schiste argileux, KD : kérogène.

(absorption at 3530 cm^{-1}, 3400 cm^{-1}, 1620 cm^{-1} and 1104 cm^{-1}) although no obvious efflorescence was visible in its proximity (Fig. 2d). All these considerations attest that the sample 6888-leaf is substantially oxidized.

4.3. S K-edge XANES spectroscopy

4.3.1. Preliminary testing

Sulfur compounds and more specifically organic sulfur may undergo redox reactions under high intensity irradiation. Therefore, the stability of maceral samples under the X-ray beam was verified by recording several consecutive spectra on the same spot with quick and standard acquisition parameters. No evolution was observed from one spectrum to another, meaning that no perceptible modification of the sulfur signature was occurring during the acquisition of the XANES spectra.

S K-edge XANES spectra were recorded on a large panel of model compounds, listed in Table 3, showing a white line maximum energy shift of approximately 13 eV from the most reduced species (ex. pyrrhotite, 2470.1 eV) to the most oxidized species (ex. dodecylsulfate, 2482.7 eV). This large shift allows for the distinction between different families of sulfur compounds based on the position of the white line maximum.

4.3.2. Un-aged Muse FL and Surmoulin shale samples

The amount of sulfur present in un-aged *Muse FL* and *Surmoulin* samples was briefly estimated by the step edge method using model samples of kaolinite charged with 0.1% w/w and 0.4%

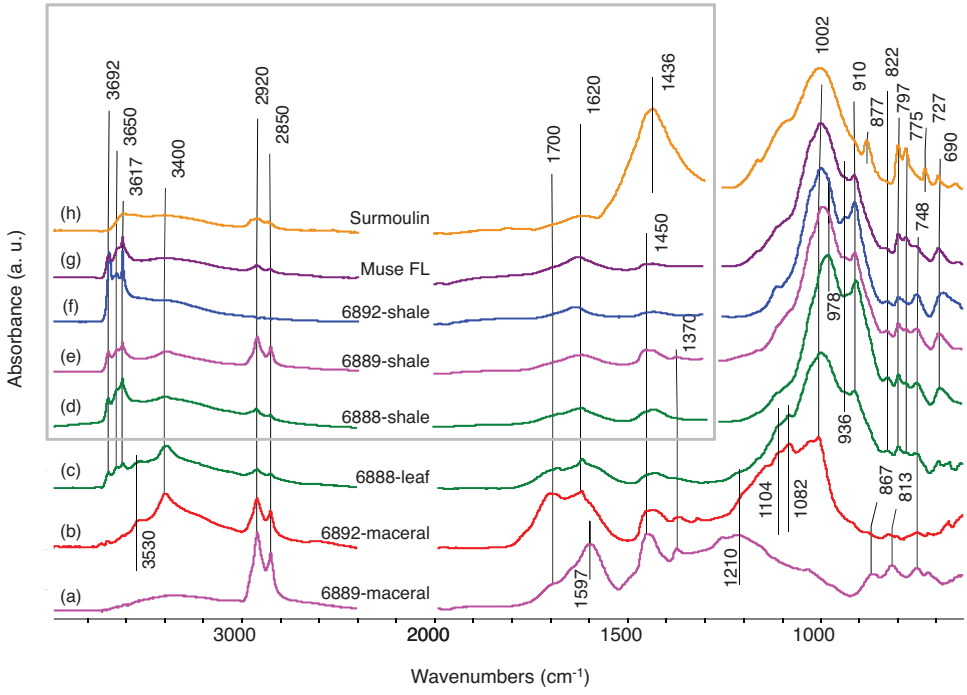

Fig. 5. FTIR spectra of shale and maceral samples; (a) 6889-maceral; (b) 6892-maceral; (c) 6888-leaf; (d) 6888-shale; (e) 6889-shale; (f) 6892-shale; (g) *Muse FL*; (h) *Surmoulin*. In the inner part of the grey rectangle, the spectra are magnified (by a factor of 2 to 3) with comparison to the outer part.
Spectres IRTF des schistes argileux et des macéraux ; (a) 6889-maceral ; (b) 6892-maceral ; (c) 6888-leaf ; (d) 6888-shale ; (e) 6889-shale ; (f) 6892-shale ; (g) Muse FL ; (h) Surmoulin. La partie des spectres dans la partie intérieure du rectangle gris est amplifiée d'un facteur 2 à 3 par rapport à la partie extérieure.

Table 3
S K-edge XANES maximum white line energy of some reference compounds. All spectra were calibrated with regard of the white line of gypsum fixed at 2482.5 eV.
Energies des seuils d'absorption de la raie K du soufre pour quelques composés de référence. Tous les spectres ont été calibrés en énergie en considérant le seuil du gypse à 2482.5 eV.

Family	Name, formula	ON	Type	Edge (eV)	Reference
Mineral sulfide	Pyrrhotite, FeS	−2	S^{2-}	2470.1	This work
	Marcasite, FeS_2	−1	S^{-}	2472.0	
	Pyrite, FeS_2	−1	S^{-}	2472.0	
Thiols	Cysteine, $(C_3H_6NO_2)SH$	−1	R-S-H	2473.1	This work
	Thiosalicylic acid, $C_6H_4(CO_2H)(SH)$	−1	R-S-H	2473.5	
Thiocyanate	Potassium Thiocyanate, KSCN	−1	NCS^{-}	2473.3	This work
Sulfur	Sulfur, S	0	S_0	2472.4	This work
Thioether	Dibenzothiophene, $(C_6H_4)_2S$	0	R-S-R	2473.6	This work
	Methionine, $(CH_3)S(C_4NH_8O_2)$	0	R-S-R	2473.4	
Disulfide	Dibenzyldisulfide, $(C_7H_7S)_2$	0	R-SS-R	2472.4	This work
	Diphenyldisulfide, $(C_6H_5S)_2$	0	R-SS-R	2472.5	
Sulfoxide	Diphenlysulfoxide, $(C_6H_5)_2SO$	2	R-SO-R	2475.9	This work
	Methionine sulfoxide, $(CH_3)SO(C_4NH_8O_2)$	2	R-SO-R	2476.1	
Sulfoxylate	Sodium formaldehyde sulfoxylate, CH_3SO_3Na	2	R-SO-O^{-}	2476.9	This work
Sulfone	Methionine sulfone, $(CH_3)SO_2(C_4NH_8O_2)$	4	R-SO_2-R	2479.6	This work
	Diphenlysulfone, $(C_6H_5)_2SO_2$	4	R-SO_2-R	2478.0	
Sulfite	Sodium sulfite, Na_2SO_3	4	$(SO_3)^{2-}$	2478.0	ID21
Thiosulfate	Ammonium thiosulfate, $(NH_4)_2S_2O_3$	−1	S^{-}	2471.8	This work
		5	$(SO_3)^{-}$	2480.6	
Sulfonate	Cysteic acid monohydrate, $(C_3H_6N_2O_2)SO_3H{\cdot}H_2O$	5	R-SO_3H	2480.6	This work
	Sodium benzene sulfonate, $(C_6H_5)SO_3Na$	5	$(RSO_3)^{-}$	2481.2	
	5-Sulfosalicylic acid, $(C_7H_5O_3)SO_3H$	5	RSO_3H	2481.4	
Disulfite	Sodium disulfite, $Na_2S_2O_5$	3	$(SO_2)^{-}$	2475.6	Tauson 2012
		5	$(SO_3)^{-}$	2478.0	
Sulfate	Jarosite, $KFe^{III}{}_3(OH)_6(SO_4)_2$	6	$(SO_4)^{2-}$	2482.8	This work
	Magnesio-copiapite, $Mg^{2+}Fe^{3+}{}_4(SO_4)_6(OH)_2{\cdot}20(H_2O)$	6	$(SO_4)^{2-}$	2482.6	
	Rozenite, $Fe^{II}SO_4{\cdot}4H_2O$	6	$(SO_4)^{2-}$	2482.5	
	Melanterite, $Fe^{II}SO_4{\cdot}7H_2O$	6	$(SO_4)^{2-}$	2482.6	
	Sodium dodecylsulfate, $(C_{12}H_{25})SO_4Na$	6	$(RSO_4)^{-}$	2482.7	

w/w of sulfur as iron sulfate. Measured concentrations of sulfur are respectively 0.4 ± 0.1% w/w for *Muse FL* and 0.15 ± 0.05% w/w for *Surmoulin*. In the case of the *Muse FL* sample, this value is comparable to the concentration of calcium (0.3 ± 0.1% w/w) and largely below that of iron (1.5 ± 0.1% w/w). In the case of Surmoulin, the concentration of sulfur is largely below those of calcium (7.6 ± 0.1% w/w) and iron (1.8 ± 0.1% w/w) (Odin et al., 2015). Also sulfur is present in low amount and could therefore be partially or totally bound to iron, calcium or organic matter.

The presence of iron sulfide was first investigated. Pyrite and marcasite show very similar spectra, with a white line maximum positioned at 2472 eV (Fig. 6, spectrum e and Table 3). This energy is significantly below those of thioethers and thiols (∼ 2473.8 eV, Table 3), thus allowing for the distinction between iron sulfides and organic sulfides. No iron sulfide was detected in the *Surmoulin* sample (Fig. 6, spectra a, g, h) while *Muse FL* samples show some small and varying amount of iron sulfide (Fig. 6, spectra f, i, j, k). These results are in good agreement with X-ray diffraction and Mössbauer analyses previously performed on these materials (Odin et al., 2015). Moreover, iron sulfide seems to be relatively unevenly distributed in the *Muse FL* shale at the scale of the beam dimension (approx. 1 mm^2).

Un-aged *Muse FL* and *Surmoulin* samples show similar spectroscopic features (Fig. 6, spectra a, b), with a main white line maximum characteristic of thiols/thioethers (2473.8 eV, Table 3). This white line is also noticeable on the asphalt and crude-oil model compounds (Fig. 6, spectra c, d) and corresponds to organic reduced sulfur compounds that are inherent of the original shale composition. Another feature situated at 2475.8 eV is observed on un-aged *Muse FL* and *Surmoulin* samples (Fig. 6, spectra a, b) as well as on asphalt and crude-oil model compounds (Fig. 6, spectra c, d). When it is of low intensity, it seems to be associated to the white line maximum at 2473.8 eV and could therefore be considered as a second edge feature of the thiol/thioether reduced sulfur compounds. However, as the intensity of this feature varies from one sample to another, it is additionally related to a different form of sulfur. The energy of this feature corresponds well with that of sulfoxides, such as diphenylsulfoxide (Table 3, 2475.9 eV) or methionine sulfoxide (Table 3, 2476.1 eV). This interpretation is consistent with previous studies (Garrett et al., 1998; Pickering et al., 2001; Sarret et al., 2002) that attributed to sulfoxides the feature close to 2476 eV measured on kerogens, asphalt and crude-oils.

Un-aged *Muse FL* and *Surmoulin* samples show an additional white line situated at 2482.5 eV and attributed to a minor presence of sulfates (Table 3). Similarly, the low intensity signal in the range 2478–2481 eV probably corresponds to minor occurrence of sulfonate, sulfite or thiosulfate (Table 3).

Some linear combination models were attempted on un-aged *Muse FL* and *Surmoulin* samples but were not giving convincing results: the region 2465–2474 eV (thiol/thioether) and 2478–2485 eV (sulfite, sulfonate, sulfate) could be relatively satisfactorily modeled considering dibenzothiophene (R-S-R), methionine (R-S-R), sulfosalicylic acid (R-SO_3H), dodecylsulfate (R-SO_4^{-}), asphalt and crude-oil "models". Yet, the region 2474–2478 eV was impossible to model with available model compounds, probably because asphalt, crude-oil and dibenzothiophene compounds were partially oxidized, thus including the presence of sulfoxide moities. However, whatever the starting components used for modeling, the final results always converged to a low amount of sulfates for un-aged *Surmoulin* and *Muse FL* samples (below 10%).

4.3.3. *Artificially aged Muse FL samples*

Artificially aged samples (Table 1) were analyzed because they showed characteristic damage during ageing, i.e., cracks and material losses (mechanical damage) or efflorescent crystalline growth mainly consisting of gypsum with some minor traces of jarosite (Raman analysis, not shown). The majority of the samples showed exhaustive efflorescence or cracks. However, one sample (*Muse FL*, 40 °C, 80% RH) showed both types of damage.

The S K-edge XANES investigation showed that these samples may be gathered in two different groups: in the first group (Fig. 6,

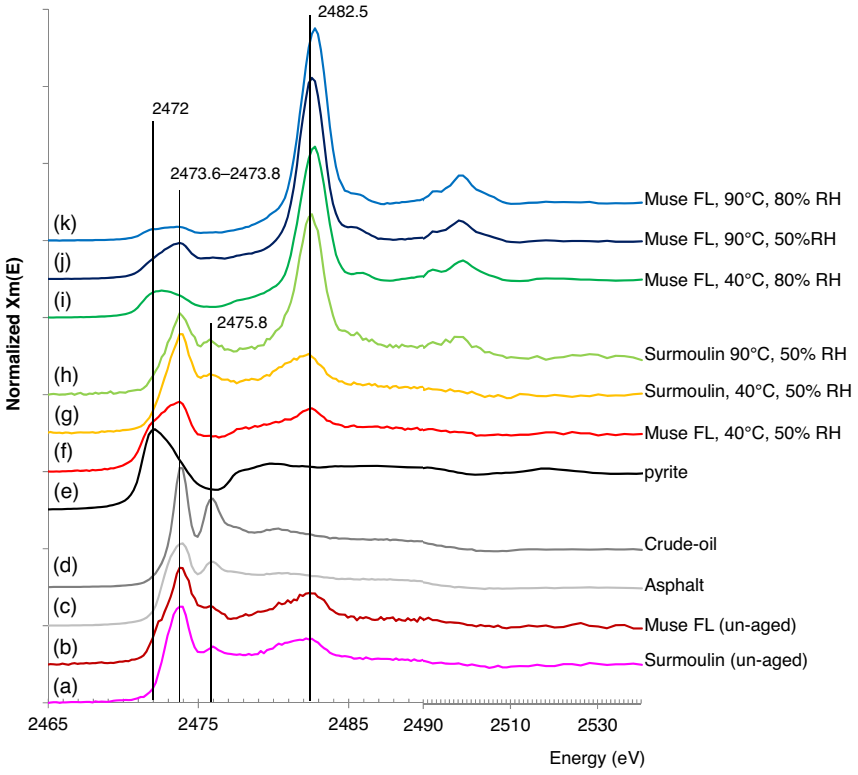

Fig. 6. S K-edge XANES spectra of newly sampled shale before and after artificial ageing; (a) *Muse FL*, un-aged; (b) *Surmoulin*, un-aged; (c) asphalt reference; (d) oil reference; (e) Pyrite reference; (f to k) artificially aged *Muse FL* and *Surmoulin* samples (see Table 1 for ageing details). Spectra are normalized and vertically translated for a better legibility of the figure.

Spectres d'absorption au seuil K du soufre des échantillons nouvellement prélevés avant et après vieillissement artificiel ; (a) Muse FL, non vieilli ; (b) Surmoulin, non vieilli ; (c) référence asphalt ; (d) référence de bitume ; (e) référence de pyrite ; (f to k) échantillons Muse FL et Surmoulin vieilli artificiellement (voir Table 1 pour le détail des vieillissements). Les spectres ont été normalisés et translatés verticalement pour une meilleure lecture.

spectra f, g), the S K-edge XANES spectra are similar to that of un-aged shale, meaning that no substantial oxidation of sulfur happened during artificial ageing. In the second group (Fig. 6 spectra h to k), an intense sulfate signal at 2482.5 eV is observed, meaning that a substantial oxidation of sulfur had occurred during artificial ageing.

4.3.4. Analysis of MNHN specimens

The samples taken from damaged specimens could be divided into two groups as well: the maceral and leaf samples (Fig. 7, spectra a, b, c) exhibit XANES spectra similar to that of un-aged shale (Fig. 6, spectrum a, b) whereas spectra obtained on the shale samples (Fig. 7, spectra d, e, f) resemble closely to that of sulfates (Fig. 7, spectra g, h).

The presence of iron sulfide is still noticeable on 6892-shale sample (Fig. 7, spectrum f) despite a strong oxidation of sulfur. This is consistent with previous Mössbauer analysis (Odin et al., 2015). Minor amount of organic sulfides are also present in this sample (as well as in the two other shale samples), meaning that sulfur is not entirely oxidized although the shale was collected more than one century ago.

4.4. Ca K-edge XANES spectroscopy

Calcium is present in *Muse FL* sample at a concentration of $0.3 \pm 0.1\%$ w/w (Odin et al., 2015). In the *6889-shale* and *6889-maceral* samples, the amount of calcium was estimated by the step edge method leading to a measure of $0.15 \pm 0.05\%$ w/w for the *6889-shale* sample and $0.015 \pm 0.01\%$ w/w for the *6889-maceral* sample.

Linear combinations of several model compounds were considered for modeling Ca K-edge XANES spectra. Calcium may have a mineral or organic origin: calcium carbonates such as dolomite, aragonite and calcite; calcium sulfates, such as gypsum or anhydrite, and finally calcium carboxylate, such as calcium acetate or calcium propionate. Model compounds of the plagioclase group were at first considered, but they never led to satisfactory results.

The spectra were modeled considering two complementary approaches. The XANES spectra of the samples were first modeled with linear combinations of spectra from model compounds. The best combination was then tested with the CCWT model. Combinations giving satisfactory results with these two model approaches were considered.

The 6889-shale sample was satisfactorily modeled with the two approaches, considering a linear combination of 38% gypsum, 18% dolomite and 44% calcium acetate (Fig. 8, spectrum b, and Fig. 9a, b). This suggests that Ca is bound to three types of second neighbors: sulfur of sulfate-type (as in gypsum), carbon of carbonate type (as in dolomite) and carbon of carboxylate type (as in acetate) with the above mentioned proportions.

The sample 6889-maceral appeared more difficult to model satisfactorily with the two approaches. A linear combination of 35% calcite and 35% anhydrite and 30% calcium propionate gave a good model of the Ca K-edge XANES spectrum (Fig. 8, spectrum c) but was less satisfactory for the wavelet approach (Fig. 9 c, d). In particular, the distant Ca-Ca pairs observed in the modeled decomposition near R~6 Å and $k = 4–5$ Å^{-1} (Fig. 9d) are not present in the wavelet decomposition of the 6889-maceral sample (Fig. 9c). These pairs are related to the 12 Ca next nearest-neighbors located near 6.4 Å in calcite (Maslen et al., 1995). Similar contributions also occur for a variety of other well-crystallized calcium carbonates (aragonite, vaterite, monohydrocalcite). Therefore, this lack of medium-range organization around Ca in the maceral is indicative of the presence

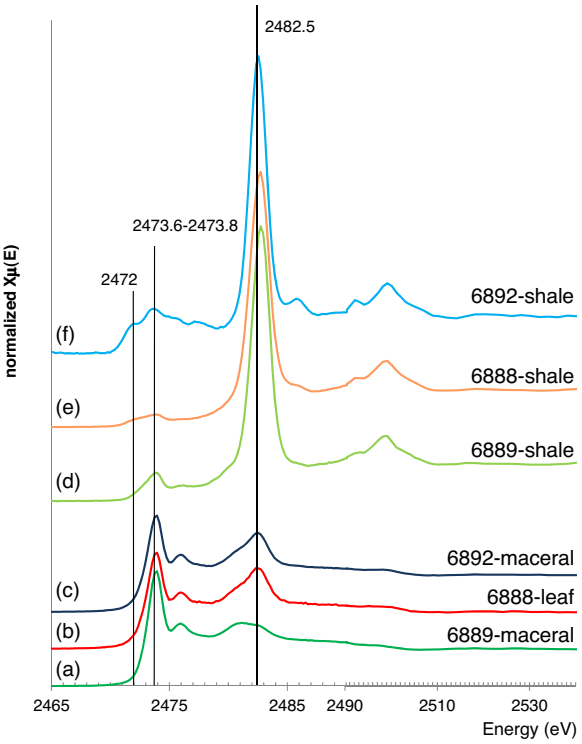

Fig. 7. S K-edge XANES spectra of MNHN specimens. (a) 6889-maceral; (b) 6888-leaf; (c) 6892-maceral; (d) 6889-shale; (e) 6888-shale; (f) 6892-shale. Spectra are normalized and vertically translated for a better legibility of the figure.
Spectres d'absorption au seuil K du soufre des spécimens MNHN. (a) 6889-maceral ; (b) 6888-leaf ; (c) 6892-maceral ; (d) 6889-shale ; (e) 6888-shale ; (f) 6892-shale. Les spectres ont été normalisés et translatés verticalement pour une meilleure lecture.

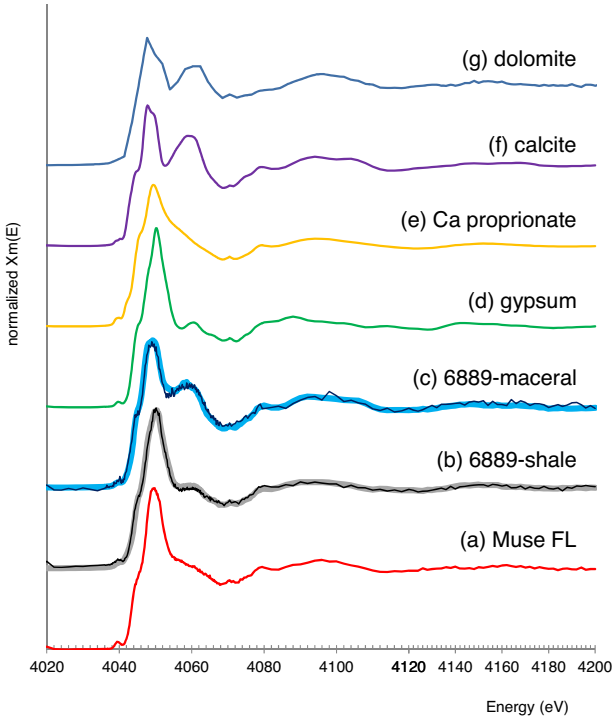

Fig. 8. Ca K-edge XANES spectra; (a) *Muse FL*, un-aged; (b) 6889-shale, experimental spectrum (thin line) and linear combination spectrum (thick line) considering 38% gypsum, 18% dolomite and 44% calcium acetate; (c) 6889-maceral, experimental spectrum (thin line) and linear combination spectrum (thick line) considering 35% calcite, 35% anhydrite and 30% calcium propionate; (d) gypsum reference; (e) calcium propionate reference; (f) calcite reference. Spectra are normalized and vertically translated for a better legibility of the figure.
Spectres d'absorption au seuil K du calcium ; (a) Muse FL, non vieilli ; (b) 6889-shale, données expérimentales (ligne mince) et combinaison linéaire (ligne épaisse) prenant en compte 38% de gypse, 18% de dolomite et 44% d'acétate de calcium ; (c) 6889-maceral, données expérimentales (ligne mince) et combinaison linéaire (ligne épaisse) prenant en compte 35% de calcite, 35% d'anhydrite et 30% de propionate de calcium ; (d) référence de gypse ; (e) référence de propionate de calcium ; (f) référence de calcite. Les spectres ont été normalisés et translatés verticalement pour une meilleure lecture.

of some disordered-carbonate-type moieties finely disseminated in this sample.

The Ca K-edge XANES spectrum of the un-aged sample of *Muse FL* (Fig. 8, spectrum a) could not be satisfactorily modeled considering our database of model compounds relevant to that peculiar geotope. However the wavelets decomposition for this Muse FL sample shows a contribution that is close to that for dolomite or a disordered-carbonate-type environment (Fig. 9e, f).

5. Discussion

5.1. Questioning the type of organic matter

The values of T_{max} measured on shale and kerogen samples by Rock-Eval pyrolysis indicate that the organic matter from Surmoulin and Muse FL samples is immature (Fig. 4a) (Espitalié et al., 1986). The investigated samples show a substantial residual oil potential because their hydrogen index (HI) values are higher than 500 mg (HC)·g^{-1} (TOC) and their oxygen index (OI) values are lower than 50 mg (CO_2)·g^{-1} (TOC) (Fig. 4a, b) (Espitalié et al., 1986).

More interesting for paleontological purpose is the use of Rock-Eval data for the classification of type I (mostly lacustrine algae), II (mostly marine plankton) and III (mostly land plants) kerogens using HI vs. OI or HI vs. T_{max} diagrams (Espitalié et al., 1985a, 1986) in a similar way as the Van Krevelen H/C vs. O/C diagram. The typical HI versus T_{max} diagram (Fig. 4a) shows that samples from *Surmoulin* and *Muse FL* are mainly situated at Type I and II kerogen domains. This result is compatible with an organic matter mainly derived from a lacustrine facies (Durand and Monin, 1980; Marteau, 1983), rich in Tasmanacea, Reinschia, pollen and humic substance (Elsass Damon, 1977).

5.2. A limited impact of on-site weathering

5.2.1. Sulfur speciation

The S K-edge XANES experiment provided bulk information on sulfur speciation and also gave an approximate value of the sulfur amount in newly excavated *Muse FL* and *Surmoulin* shale. Both contain low amounts of sulfur ($0.4 \pm 0.1\%$ w/w for *Muse FL* and $0.15 \pm 0.05\%$ w/w for *Surmoulin*). In *Surmoulin* shale, sulfur exclusively corresponds to organic sulfide compounds (thioether or thiols) relatively evenly distributed in the shale at the scale of the beam size (1 mm^2) whereas in *Muse FL* shale, it is also present as unevenly distributed pyrite. Yet in both shale materials, a small proportion of sulfur is detected as sulfoxide, sulfonate and sulfate (< 10%). Maximal cautions were taken to avoid exposure to oxygen between excavation and analysis. Some of these proved to be unnecessary as newly excavated shale could be exposed to oxygen for several hours without inducing a notable sulfur oxidation. It is also believed that the low amounts of sulfoxide, sulfonate and sulfate were already present on site at the moment of the sample collection. Sulfonate and sulfate species correspond unambiguously to weathering phenomena occurring on site. The relationship between sulfoxide and weathering phenomena appears more questionable as sulfoxide are sometimes detected as primary components of S rich kerogens, for instance in the Kashpir Oil shale (Riboulleau et al., 2000). These shale however have the particularity to be very rich in oxygen (O/C = 0.2),

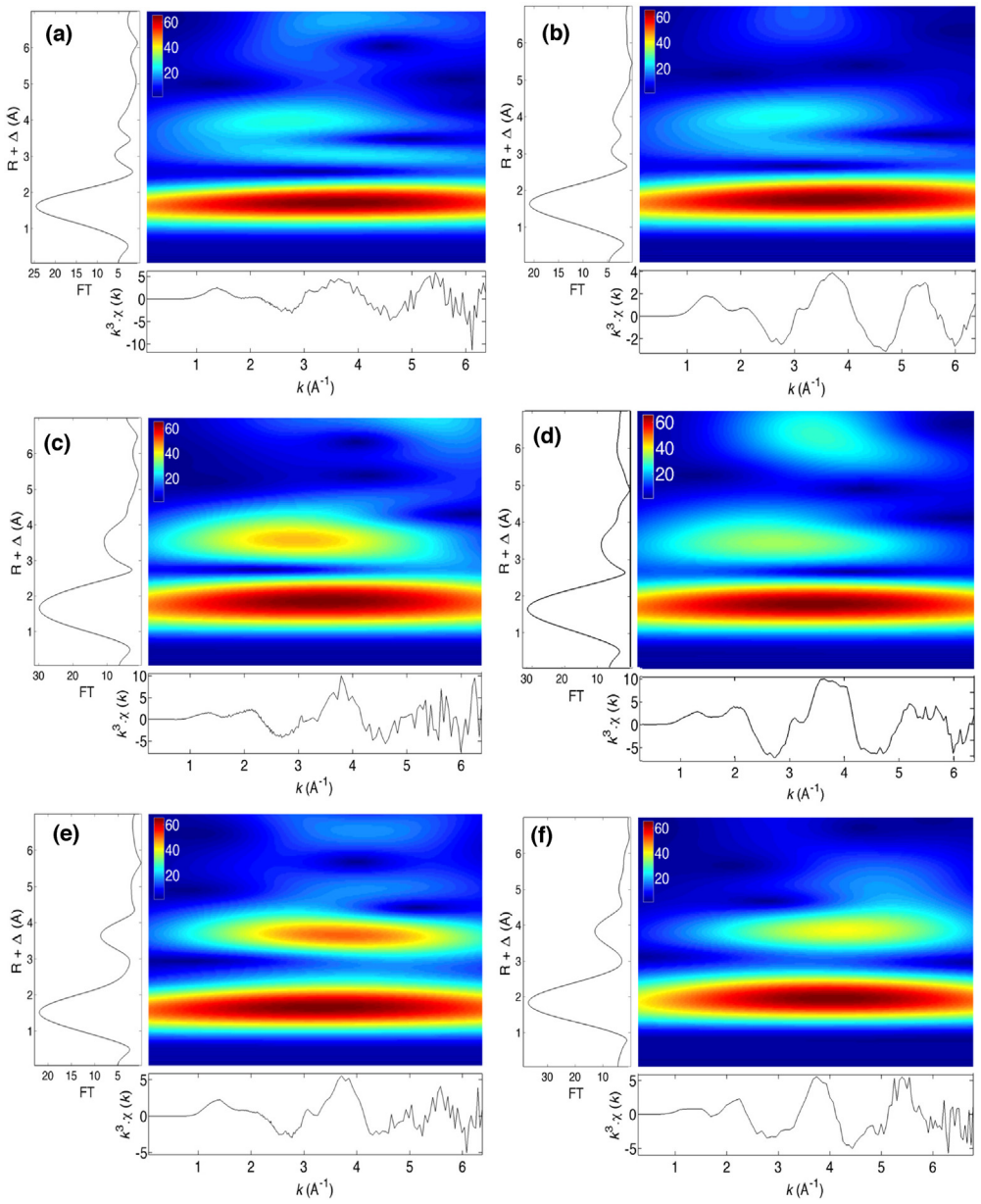

Fig. 9. Continuous Cauchy Wavelet Transform modeling of Ca K-edge XANES data; (a) 6889-shale; (b) model of 6889-shale considering a linear combination of 38% gypsum, 18% dolomite and 44% calcium acetate; (c) 6889-vitrinite; (d) model of 6889-vitrinite considering a linear combination of 35% calcite, 35% anhydrite and 30% calcium propionate; (e) Muse FL; (f) dolomite. The graph on the left represents the Fourier Transform modulus (FT) versus the R + Δ parameter (uncorrected interatomic phase shift S-X distance). The central image is a three dimensions representation of the XANES data. It corresponds to the CCWT modulus, versus the wavenumber k (horizontal axis) and the parameter R + Δ (vertical axis).

Modélisation par transformées d'ondelettes de Cauchy des mesures d'absorption au seuil K du calcium; (a) 6889-shale; (b) modélisation de 6889-shale considérant une combinaison linéaire de 38 % de gypse, 18 % de dolomite et 44 % d'acétate de calcium ; (c) 6889-vitrinite ; (d) modélisation de 6889-vitrinite considérant une combinaison linéaire de 35 % de calcite, 35 % d'anhydrite et 30 % de propionate de calcium ; (e) Muse FL ; (f) dolomite. Le graphe de gauche représente le module de la transformée de Fourier (FT) en fonction du paramètre R + Δ (décalage de phase non corrigé de la distance interatomique S-X). L'image centrale est une représentation en trois dimensions des données XANES. Elle correspond au module de la transformée en ondelette, en fonction du nombre d'onde k (axe horizontal) et du paramètre R + Δ (axe vertical).

which is not the case of our samples (O/C in the range 0.001 to 0.016). Sulfoxide species are moreover commonly found as oxidation by-products of bitumen and not necessary present as primary products (Sarret et al., 1999, 2002). These considerations suggest that sulfoxide species are more probably present as weathering by-products even if their occurrence as primary products cannot be totally excluded. The impact of this weathering appears limited, if not totally negligible, since if affects a minor proportion of sulfur.

5.2.2. Organic matter

On-site weathering may not only have an impact on sulfide species but also on organic matter and both effects are not necessarily correlated. Organic matter weathering affects Rock-Eval parameters, leading in particular to an underestimation of HI values and overestimation of OI values (Espitalié et al., 1985a; Espitalie et al., 1980; Katz, 1983; Peters, 1986). The impact of weathering on *Muse FL* and *Surmoulin* samples appears however negligible because the measured values of OI are low on all tested samples.

5.3. Evolution of speciation versus ageing

5.3.1. Sulfur speciation

Maceral samples found on MNHN specimens belong to the group of vitrinite. They exhibit an S speciation (Fig. 7, spectra a and d) similar to that found in newly excavated shale (Fig. 6, spectra a and b) with a large proportion of reduced organic sulfide species.

Despite showing the same sulfur speciation as un-aged shale, the maceral appears to be less sensitive to sulfur oxidation than shale. This is demonstrated by the comparison of the XANES spectra collected on specimens sampled more than one century ago (Fig. 7, spectra a, b and c): 6889-maceral, 6888-leaf and 6892-maceral samples mainly contain organic sulfides (with a minor proportion of sulfates, and probably sulfonates or sulfites) whereas 6888-shale, 6889-shale and 6892-shale samples mainly contain sulfates (with only a small amount of sulfides). This differing sensitivity to oxidation is related to the differing porosity of these two materials. Indeed, the porosity of shale, measured by mercury intrusion porosimetry, ranges from 7 to 10% v/v (Odin et al., 2015) whereas similar measurements performed on the 6889-maceral sample gave a value of 0% (not shown).

Sulfates resulting from sulfide oxidation in shale may bind iron, calcium, or organic matter. Gypsum and jarosite are indeed detected by X-ray diffraction on shale fractions of specimen 6888 and 6889 (Odin et al., 2014). The S K-edge XANES white line of jarosite is positioned at 2482.8 eV (Table 3) whereas that of gypsum is at 2482.5 eV. The varying relative amount of jarosite/gypsum formed in the shale during ageing explains the ~0.3 eV shift observed in the sulfate white line and the sulfate feature variation observed near 2485.8 eV among the shale samples (Figs. 6 and 7).

Remarkably, *Muse FL* shale samples still contain some amount of pyrite and organic sulfide after artificial ageing (Fig. 6, spectra f, i, j, k), meaning that sulfur oxidation is incomplete. This is also true for the shale fraction of MNHN specimens (Fig. 7, spectra d, e, f). As pyrite is unevenly distributed in shale, it appears difficult to determine which of the pyrite or organic sulfide is more prone to oxidation.

5.3.2. Calcium speciation

Although most vitrinite studies focus on organic composition, it has been reported that vitrinite could contain some amount of calcium (< 0.4%) (Ward et al., 2007). This point is confirmed on the maceral of specimen 6889. Moreover, Ca K-edge XANES measurements showed that this calcium is partly related to poorly ordered carbonates.

This consideration prevails for shale as well: in the *Muse FL* sample, calcium has also, at least partly, a carbonate origin as the *6889-shale* sample was well modeled considering dolomite as model compound. In addition to carbonates, the Ca K-edge models of the vitrinite and shale fractions of specimen 6889, include some carboxylate moieties, which are obviously related to the organic part of these materials. In the vitrinite sample, these moities participate to the 1700 cm^{-1} absorption peak observed on FTIR spectra (Fig. 5, spectrum a). The occurrence of carboxylic acids in soil organic matter is often mentioned in the literature, but that of carboxylate salts is much less studied. It was however demonstrated that these salts could be present in lignites (Miller and Given, 1986, 1987), marine source rock (Liu et al., 2013) and shale (Chong and McKay, 1984). The present study shows that they can also be present in macerals.

Calcium sulfates are detected in these materials, but are considered as degradation phases resulting from sulfide oxidation. This is in particular the case of the highly oxidized shale fraction of specimen 6889 that was well modeled considering gypsum as model compound. This also prevails when sulfide oxidation is limited as for the maceral of specimen 6889. On this sample, there is approximately one order of magnitude between the concentration of sulfur (0.15 ± 0.05% w/w) and that of calcium (0.015 ± 0.01% w/w). The small amount of sulfate formed by oxidation also combines with calcium. As a result, a substantial proportion of calcium is bound to sulfates (Ca K-Edge XANES measurements).

5.4. Comparing the effect of natural (museal) and artificial ageing

The occurrence of sulfates in the matrix of the artificially aged *Muse FL* shale samples (Fig. 6, spectra h, i, j, k) is consistent with the growth of gypsum efflorescence visible on the shale surface (Table 1). In addition, the two shale samples in which sulfur is not oxidized (Fig. 6, spectra f, g) correspond to the two samples of Table 1 that are not affected by efflorescence growth but by mechanical damage only (*Surmoulin* and *Muse FL* aged at 50 °C and 50% RH).

First, this means that there is some correlation between the oxidation of sulfur in the inner part of the shale matrix (measured by S K-edge XANES) and the efflorescence growth observed on the surface of shale. Second, this means that the flaking artificially induced on shale samples is not related to sulfur oxidation and sulfate efflorescence. The cause of the mechanical damage is more likely related to the intrinsic physical properties of the shale. A possible explanation would be physical stress because of temperature variations (when the samples are removed from the laboratory oven to be photographed). This conclusion, however, contrasts with the visual observations made on MNHN specimens where the shale is obviously flaking because of the growth of iron sulfate efflorescence (Fig. 2c). Indeed, on these specimens, there is no obvious mechanical damage without sulfate efflorescence.

Second, soft ageing conditions (40 °C and 50% RH) failed to induce oxidation of sulfides within a reasonable time frame (15 weeks). In contrast, more severe conditions (90 °C and/or 80% RH) were efficient in oxidizing sulfur within the shale matrix in a way that is comparable to that of natural ageing occurring in a museum environment (similar S K-edge XANES spectra). Still the efflorescence observed on artificially aged samples mainly consists of disseminated spots of gypsum. These are sometimes visible on damaged specimens but they do not grow preferentially nearby the fossil. They remain disseminated and hardly perceptible by the naked eye and are thus considered as damage of secondary importance. Unlike gypsum, iron (II) sulfates (rozenite and szomolnokite) growth on MNHN specimens is considered as damage of primary importance. It leads to proliferous efflorescence covering the shale and largely overlapping the fossil shape, thus comprising its paleontological value. This type of efflorescence was not reproduced in laboratory conditions on our sample set. Artificial ageing conditions should not be reappraised as they succeeded in provoking sulfur oxidation. It is probably of more interest to revise the choice of the sample set as they did not contain visible traces of fossil remains.

6. Conclusion

In the field of Museum conservation, pyrite is usually presented as the main cause of shale degradation. However, S K-edge XANES measurements performed in this study show that organic sulfides are abundant in organic matter and are also subject to oxidation. This second type of oxidation leads to the formation of sulfoxides (R-SO-R), sulfonates (R-SO_3^-) and sulfates (SO_4^{2-} and possibly RSO_4^-). Sulfones (R-SO_2-R) that are expected as intermediate oxidation products were not detected, meaning that they are probably highly reactive.

S K-edge XANES signatures are identical for maceral and newly sampled shale. These correspond to thioether or thiol compounds

while sulfates are dominantly found in the shale fraction of damaged specimens. Sulfide compounds present in vitrinite appear therefore highly stable while similar compounds present in shale are easily oxidized. This different behavior probably corresponds to the different porosity of the two materials, which makes oxygen and water either more or less accessible.

Newly excavated shale samples show two distinct behaviors after 15 weeks of artificial ageing: when conditions are "soft" (50 °C and 50% RH), no visible efflorescence is observed whereas the sulfides present in the inner part of shale remain unoxidized. When conditions are more drastic (90 °C and/or 80% RH), shale is damaged by sulfate efflorescence (mainly consisting of gypsum) and the sulfides present in the inner part of shale are almost entirely transformed into a mixture of iron and calcium sulfates. This second behavior is consistent with the museal evolution of damaged specimens, which are housed in drawers for centuries. However, these artificial ageing experiments did not provoke large efflorescence of iron (II) sulfates as the ones observed on MNHN specimens. Further investigations remain, to this respect, necessary.

Disclosure of interest

The authors declare that they have no conflicts of interest concerning this article.

Acknowledgement

This work was conducted within a PhD work that was supported by a doctoral school grant of the Museum national d'Histoire naturelle, Paris, France. We acknowledge SOLEIL for provision of synchrotron radiation facilities (Proposals ID "20130462" and "20110189") and we would like to thank Nicolas Trcera, Pierre Lagarde and Anne Marie Flanck for assistance in using beamline LUCIA.

This work was realized in partnership with the Palaeontological Collection Management Unit, Collection Department, National Museum of Natural History (Paris, France). We also would like to thank MM. Hervé Lelièvre, Olivier Bethoux, Sebastien Steyer, Jean Dejax and Dario de Franceschi for their advice and assistance.

References

Almkvist, G., Boye, K., Persson, I., 2010. K-edge XANES analysis of sulfur compounds: an investigation of the relative intensities using internal calibration. Journal of Synchrotron Radiation 17, 683–688.

Behar, F., Beaumont, V., Penteado, H.L.D.B., 2001. Rock-Eval 6 Technology: Performances and Developments. Oil & Gas Science and Technology. Revue de l'Institut Francais du Pétrole 56, 111–134.

Boye, K., Almkvist, G., Nilsson, S.I., Eriksen, J., Persson, I., 2011. Quantification of chemical sulphur species in bulk soil and organic sulphur fractions by S K-edge XANES spectroscopy. European Journal of Soil Science 62, 874–881.

Chabard, D., Passaqui, J.P., 2006. L'essence Autunoise, un carburant national. Museum d'Histoire Naturelle, Autun, pp. 104.

Chandra, A.P., Gerson, A.R., 2010. The mechanisms of pyrite oxidation and leaching: a fundamental perspective. Surface Science Reports 65, 293–315.

Chen, Y., Mastalerz, M., Schimmelmann, A., 2012. Characterization of chemical functional groups in macerals across different coal ranks via micro-FTIR spectroscopy. International Journal of Coal Geology 104, 22–33.

Chong, S.L., McKay, J.F., 1984. Extractable metal-salts of carboxylic acids in green river oil shale. Fuel 63, 303–309.

Durand, B., Monin, J.C., 1980. Elemental analysis of kerogens (C, H, O, N, S, Fe). In: Durand, B. (Ed.), Kerogen, insoluble organic matter from sedimentary rocks. Technip, Paris, pp. 113–162.

Durand, B., Nicaise, G., 1980. Procedure for kerogen isolation. In: Durand, B. (Ed.), Kerogen, insoluble organic matter from sedimentary rocks. Technip, Paris, pp. 35–53.

Elsass Damon, F., 1977. Les "schistes bitumineux" du bassin d'Autun : pétrographie, minéralogie, cristallochimie, pyrolise [PhD thesis]. Université Pierre et Marie Curie, Paris, pp. 93 (unpublished).

Espitalié, J., Deroo, G., Marquis, F., 1985a. La pyrolyse Rock-Eval et ses applications. Deuxième partie. Oil & Gas Science and Technology. Revue de l'Institut Francais du Pétrole 40, 755–784.

Espitalié, J., Deroo, G., Marquis, F., 1985b. La pyrolyse Rock-Eval et ses applications. Première partie. Oil & Gas Science and Technology. Revue de l'Institut Francais du Pétrole 40, 563–579.

Espitalié, J., Deroo, G., Marquis, F., 1986. La pyrolyse Rock-Eval et ses applications. Troisième partie. Oil & Gas Science and Technology. Revue de l'Institut Francais du Pétrole 41, 73–89.

Espitalie, J., Madec, M., Tissot, B., 1980. Role of Mineral Matrix in Kerogen Pyrolysis - Influence on Petroleum Generation and Migration. AAPG Bulletin – American Association of Petroleum Geologists 64, 59–66.

Fellowes, D., Hagan, P., 2003. Pyrite oxidation: the conservation of historic shipwrecks and geological and palaeontological specimens. Reviews in Conservation 4, 26–38.

Gand, G., Steyer, J.-S., Chabard, D., 2010. Reprise de fouilles paléontologiques dans un gîte bourguignon célèbre : les "schistes bitumineux" de l'Autunien de Muse (Bassin d'Autun). Revue Scientifique Bourgogne Nature 12, 10–29.

Garrett, R.M., Pickering, I.J., Haith, C.E., Prince, R.C., 1998. Photooxidation of crude oils. Environmental Science & Technology 32, 3719–3723.

Heidel, C., Tichomirowa, M., 2011. The isotopic composition of sulfate from anaerobic and low oxygen pyrite oxidation experiments with ferric iron - New insights into oxidation mechanisms. Chemical Geology 281, 305–316.

Howie, F.M.P., 1977. Pyrite and conservation part 2. Geological Curators Group Newsletter 10, 497–512.

Katz, B.J., 1983. Limitation of rock eval pyrolysis for typing organic matter. Organic Geochemistry 4, 195–199.

Li, W., Zhu, Y., Chen, S., Zhou, Y., 2013. Research on the structural characteristics of vitrinite in different coal ranks. Fuel 107, 647–652.

Liu, Q., Jin, Z., Liu, W., Lu, L., Meng, Q., Tao, Y., Han, P., 2013. Presence of carboxylate salts in marine carbonate strata of the Ordos Basin and their impact on hydrocarbon generation evaluation of low TOC, high maturity source rocks. Science China-Earth Sciences 56, 2141–2149.

Manceau, A., Nagy, K.L., 2012. Quantitative analysis of sulfur functional groups in natural organic matter by XANES spectroscopy. Geochimica et Cosmochimica Acta 99, 206–223.

Marteau, P., 1983. Le bassin permo-carbonifère d'Autun : stratigraphie, sédimentologie et aspects structuraux [PhD thesis]. Department of Geology, Université de Bourgogne, Dijon, pp. 188.

Maslen, E.N., Streltsov, V.A., Streltsova, N.R., Ishizawa, N., 1995. Electron density and optical anisotropy in rhombohedral carbonates. III. Synchrotron X-ray studies of CaCO3, MgCO3 and MnCO3. Acta Crystallographica B 51, 929–939.

Mikhlin, Y., Tomashevich, Y., 2005. Pristine and reacted surfaces of pyrrhotite and arsenopyrite as studied by X-ray absorption near-edge structure spectroscopy. Physics and Chemistry of Minerals 32, 19–27.

Miller, R.N., Given, P.H., 1986. The association of major and trace inorganic elements with lignites. I. Experimental approach and study of a North Dakota lignite. Geochimica et Cosmochimica Acta 50, 2033–2043.

Miller, R.N., Given, P.H., 1987. The association of major, minor and trace inorganic elements with lignites, 2. Minerals, and major and minor element profiles, in 4 seams. Geochimica et Cosmochimica Acta 51, 1311–1322.

Munoz, M., Argoul, P., Farges, F., 2003. Continuous Cauchy wavelet transform analyses of EXAFS spectra: a qualitative approach. American Mineralogist 88, 694–700.

Murphy, R., Strongin, D.R., 2009. Surface reactivity of pyrite and related sulfides. Surface Science Reports 64, 1–45.

Newman, A., 1998. Pyrite oxidation and museum collections: a review of theory and conservation treatments. The Geological Curator 6, 363–371.

Odin, G.P., Cabaret, T., Mertz, J.D., Menendez, B., Etienne, L., Wattiaux, A., Rouchon, V., 2015. Alteration of fossil-bearing shale (Autun Basin, France; Permian), part I: characterizing iron speciation and its vulnerability to weathering by combined use of Mössbauer spectroscopy, X-ray diffraction, porosimetry and permeability measurements. Annales de Paléontologie 101 (2), 11 p.

Odin, G.P., Vanmeert, F., Janssens, K., Lelièvre, H., Mertz, J.-D., Rouchon, V., 2014. Accelerated ageing of shales of palaeontological interest: impact of temperature conditions. Annales de Paléontologie 100, 137–149.

Peters, K.E., 1986. Guidelines for evaluating petroleum source rock using programmed pyrolysis. AAPG Bulletin – American Association of Petroleum Geologists 70, 318–329.

Petit, S., Righl, D., Madejova, J., 2006. Infrared spectroscopy of NH(4)(+)-bearing and saturated clay minerals: a review of the study of layer charge. Applied Clay Science 34, 22–30.

Pickering, I.J., George, G.N., Yu, E.Y., Brune, D.C., Tuschak, C., Overmann, J., Beatty, J.T., Prince, R.C., 2001. Analysis of sulfur biochemistry of sulfur bacteria using X-ray absorption spectroscopy. Biochemistry 40, 8138–8145.

Post, J.L., Borer, L., 2002. Physical properties of selected illites, besidellites and mixed-layer illite-beidellites from southwestern Idaho, and their infrared spectra. Applied Clay Science 22, 77–91.

Prietzel, J., Thieme, J., Neuhausler, U., Susini, J., Kogel-Knabner, I., 2003. Speciation of sulphur in soils and soil particles by X-ray spectromicroscopy. European Journal of Soil Science 54, 423–433.

Ravel, B., Newville, M., 2005. ATHENA and ARTEMIS: data analysis for X-ray absorption spectroscopy using IFEFFIT. Journal of Synchrotron Radiation 12, 537–541.

Riboulleau, A., Derenne, S., Sarret, G., Largeau, C., Baudin, F., Connan, J., 2000. Pyrolytic and spectroscopic study of a sulphur-rich kerogen from the "Kashpir oil shales" (Upper Jurassic, Russian platform). Organic Geochemistry 31, 1641–1661.

Rimstidt, J.D., Vaughan, D.J., 2003. Pyrite oxidation: a state-of-the-art assessment of the reaction mechanism. Geochimica et Cosmochimica Acta 67, 873–880.

Rosso, K.M., Vaughan, D.J., 2006. Reactivity of Sulfide Mineral Surfaces. In: Vaughan, D.J. (Ed.), Reviews in mineralogy and geochemistry: sulfide mineralogy and geochemistry. Mineralogical Society of America, pp. 557–607.

Rouchon, V., Badet, H., Belhadj, O., Bonnerot, O., Lavédrine, B., Michard, J.G., Miska, S., 2012. Raman and FTIR spectroscopy applied to the conservation report of paleontological collections: identification of Raman and FTIR signatures of several iron sulfate species such as ferrinatrite and sideronatrite. Journal of Raman Spectroscopy 43, 1265–1274.

Sarret, G., Connan, J., Kasrai, M., Bancroft, G.M., Charrie-Duhaut, A., Lemoine, S., Adam, P., Albrecht, P., Eybert-Berard, L., 1999. Chemical forms of sulfur in geological and archeological asphaltenes from Middle East, France, and Spain determined by sulfur K- and L-edge X-ray absorption near-edge structure spectroscopy. Geochimica et Cosmochimica Acta 63, 3767–3779.

Sarret, G., Mongenot, T., Connan, J., Derenne, S., Kasrai, M., Bancroft, G.M., Largeau, C., 2002. Sulfur speciation in kerogens of the Orbagnoux deposit (Upper Kimmeridgian, Jura) by XANES spectroscopy and pyrolysis. Organic Geochemistry 33, 877–895.

Sayin, M., Grafvonreichenbach, H., 1979. X-ray and Infrared Investigations of a Synthetic Dioctahedral Vermiculite Saturated with Alkali and Alkaline-earth Cations. Clay Minerals 14, 211–228.

Schoonen, M.A.A., Harrington, A.D., Laffers, R., Strongin, D.R., 2010. Role of hydrogen peroxide and hydroxyl radical in pyrite oxidation by molecular oxygen. Geochimica et Cosmochimica Acta 74, 4971–4987.

Van Hullebusch, E., Rossano, S., Farges, F., Lenz, M., Labanowski, J., Lagarde, P., Flank, A.M., Lens, P., 2009. Sulfur K-edge XANES spectroscopy as a tool for understanding sulfur chemical state in anaerobic granular sludge. Journal of Physics Conference Series 190, 012184.

Van der Marel, H.W., Krohmer, P., 1969. O-H Stretching vibrations in kaolinite and related minerals. Contributions to Mineralogy and Petrology 22, 73–82.